

Towards large-scale restricted active space calculations inspired by the Schmidt decomposition

Gergely Barcza,^{1,2,3} Miklós Antal Werner,^{4,5} Gergely Zaránd,^{4,5} Anton Pershin,¹ Zsolt Benedek,^{1,3} Örs Legeza,^{1,6,7,*} and Tibor Szilvási³

¹Wigner Research Centre for Physics, H-1525, Budapest, Hungary

²Department of Physics of Complex Systems, ELTE Eötvös Loránd University, H-1117, Budapest, Hungary

³Department of Chemical and Biological Engineering, The University of Alabama, Tuscaloosa, AL-35487, USA

⁴Department of Theoretical Physics, Institute of Physics, Budapest University of Technology and Economics, H-1111 Budapest, Hungary

⁵MTA-BME Quantum Dynamics and Correlations Research Group, H-1111 Budapest, Hungary

⁶Fachbereich Physik, Philipps-Universität Marburg, 35032 Marburg, Germany

⁷Institute for Advanced Study, Technical University of Munich, Lichtenbergstrasse 2a, 85748 Garching, Germany

(Dated: December 1, 2022)

Abstract: We present an alternative, memory-efficient, Schmidt decomposition-based description of the inherently bipartite restricted active space (RAS) scheme, which can be implemented effortlessly within the density matrix renormalization group (DMRG) method via the dynamically extended active space procedure. Benchmark calculations are compared against state-of-the-art results of C₂ and Cr₂, which are notorious for their multi-reference character. Our results for ground and excited states together with spectroscopic constants demonstrate that the proposed novel approach, dubbed as DMRG-RAS, which is variational and free of uncontrolled method errors, has the potential to outperform conventional methods for strongly correlated molecules.

I. INTRODUCTION

The accurate theoretical description of molecular electronic structures is provided by the solution of the time-independent Schrödinger equation. In the Born–Oppenheimer approximation, the second quantized representation of the corresponding ab initio Hamiltonian¹ reads

$$\hat{H} = \sum_{ij,\sigma} t_{ij} \hat{a}_{i\sigma}^\dagger \hat{a}_{j\sigma} + \frac{1}{2} \sum_{ijkl,\sigma\sigma'} V_{ijkl} \hat{a}_{i\sigma}^\dagger \hat{a}_{j\sigma'}^\dagger \hat{a}_{k\sigma'} \hat{a}_{l\sigma} + E_{\text{nuc}} \quad (1)$$

with system specific one- and two-electron integrals, t_{ij} , and V_{ijkl} , respectively. Here, operators $\hat{a}_{i\sigma}^\dagger$ and $\hat{a}_{i\sigma}$ create and annihilate one electron with σ spin projection in molecular orbital $i \in \{1, \dots, L\}$. The dimension of the complete associated computational basis, Φ , increases exponentially with spin-orbital size L , i.e., 4^L . Considering available spatial symmetries and the conservation of particle and spin quantum numbers, the effective rank of the problem still shows a binomial growth for increasing L . Therefore, the exact solution based on the full configuration interaction (FCI) method on current classical computers is restricted up to around 20 orbitals.²

One protocol that aims to keep the problem of n_e electrons computationally feasible is the complete active space (CAS) scheme^{3–5} which restricts the large configuration space to an effective subset spanned by given $L_{\text{CAS}} \leq L$ orbitals. As illustrated in Fig. 1, the protocol classifies the set of canonical molecular orbitals into three categories: core, active, and virtual. The core and virtual orbitals are kept on the Hartree-Fock level and filled with $n(\Phi_{\text{core}}) = n_{\text{core}}$ and zero electrons, respec-

tively. Note that in this context core orbitals refer to inactive occupied orbitals in general. The active orbitals are populated with the rest of electrons, $n_a = n_e - n_{\text{core}}$, minimizing the energy. The corresponding determinantal space formally reads

$$\Phi_{\text{CAS}} \equiv \hat{P}_{\text{CAS}} \Phi = \{\Phi_{\text{core}} \Phi_A \in \Phi \mid n(\Phi_A) = n_a\} \quad (2)$$

where the independent conservation of spin channels is not explicitly noted for the sake of brevity. Here, Φ_{core} denotes the string of occupied modes corresponding to the core orbitals while $\Phi_A \in \Phi_A$ iterates on the set of mode configurations given within the subspace of active orbitals, and the operator \hat{P}_{CAS} projects onto the CAS subspace.

In practical simulations of large systems, a subspace of $L_{\text{CAS}} \ll L$ orbitals is selected to focus on the description of states with strong (static) correlations, i.e., excited configurations that have largest contribution to the ground state. Even though static correlations characterizes the principal features of the electronic states, the contribution of intractable number of excited configurations with small weights, known as dynamical effects, can also be crucial to provide an accurate theoretical description that agrees with experimental data.^{6,7} Although CAS level solutions can be combined with lower-level methods, e.g., self-consistent field theory, or coupled cluster method, which aim to provide a balanced description of correlation effects^{8,9} these attempts often have unfavorable drawbacks and limitations.

In the tailored coupled cluster (TCC) method^{10–13}, for example, the full orbital space is split into two parts, CAS and external (EXT). An accurate solution of the CAS is used to obtain a single reference-like wave func-

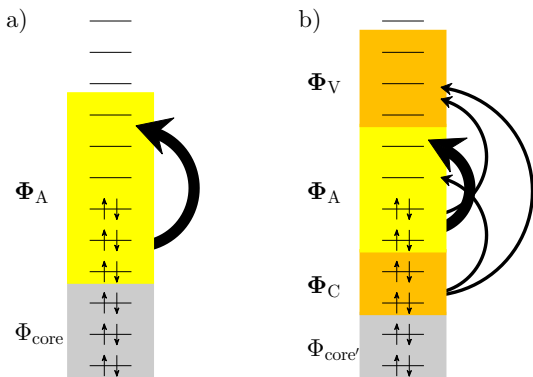


FIG. 1. Schematic illustration of the CAS and RAS concepts. (a) In the CAS scheme the occupation of modes can only change for the active orbitals (A) while occupation of the core and virtual orbitals is frozen. (b) In the RAS scheme, in addition to active orbitals some virtual (V) and core (C) orbitals can also be excited with restrictions: the maximal number of particle excitations in these orbitals is r .

tion for a truncated CC approach to recover a large fraction of the missing dynamical correlations. In spite of the great success of the tailored methods^{14–17}, their uncontrollable errors often hinder their application in black-box manner^{18,19}. In order to tackle these problems within the formalism of coupled cluster theory, besides geminal-based single-reference solutions²⁰, its computationally challenging multireference extensions have also been proposed^{21–24}. As an alternative approach based on the generalization of the active space scheme^{25,26}, the restricted active space (RAS) approach²⁷, which is practically analogue to the uncontracted multi-reference configuration interaction²⁴, has also gained significant attention²⁸.

In this work, we aim to bring the RAS scheme to a higher level by cross fertilizing it with concept of the Schmidt decomposition and with powerful numerical methods based on tensor product approximation, like the density matrix renormalization group (DMRG) algorithm²⁹. Note that similar concept has also been

proposed by grouping orbitals according to various schemes^{30–32}.

Our paper is organized as follows: In Sec. II we define the main aspects of the RAS approach and present a novel combination of it with Schmidt decomposition. In Sec. III we discuss implementation details within the framework of the DMRG method, focusing on the modifications of the dynamically extended active space (DEAS) procedure and internal basis contractions based on von Neumann entropy. In Sec. IV we demonstrate the efficiency of our new approach for the C_2 and Cr_2 molecules. In Sec. V we summarize the results and present the conclusions of our work.

II. THEORETICAL BACKGROUND

A. Restricted active space (RAS) approach

Conceptually, RAS^{27,33} enhances CAS description by distinguishing two additional subsets of orbitals which define the excitable core (Φ_C) and virtual (Φ_V) configurational spaces in addition to Φ_A . (Note that the literature^{5,33} also refers to configurational sets Φ_C , Φ_A and Φ_V generated on orbital subsets C, A and V as RAS1, RAS2 and RAS3 spaces, respectively.) In the C and V subsets of orbitals we allow a total of r (particle) excitations at most as sketched in Fig. 1. While this restriction in the C and V spaces drastically reduces the computational dimension, the method can still describe the (weak) dynamical correlations and account for their energy contribution. In the reference (Slater) configuration the orbitals in space Φ_C are completely filled with n_c electrons, and the active orbitals are occupied by $n_e - n_{core'} - n_c$ particles, where $n_{core'}$ is the number of electrons in the low-energy frozen orbitals, $\Phi_{core'}$, that are still kept at the Hartree-Fock level.

The formally considered $\Phi_C \in \Phi_C$, $\Phi_V \in \Phi_V$ strings of modes are defined within the domain of the core and the virtual subspaces and constrained by maximal r electronic excitations. The associated determinantal space of the RAS scheme we define as

$$\Phi_{RAS[r]} \equiv \hat{P}_{RAS[r]} \Phi = \{ \Phi_{core'} \Phi_C \Phi_A \Phi_V \in \Phi \mid n(\Phi_C \Phi_A \Phi_V) = n_e - n_{core'} \wedge \mathcal{C}(n_c - n(\Phi_C), n(\Phi_V), r) \}, \quad (3)$$

where $\mathcal{C}(n_c - n(\Phi_C), n(\Phi_V), r)$ denotes a condition for the allowed number of holes in the C orbitals, $n_c - n(\Phi_C)$, and for the permitted number of electrons in the V virtual space, $n(\Phi_V)$, according to restrictions based on r . In particular, it is typical to constrain the Φ_C and Φ_V occupations by requiring $n_c - n(\Phi_C) \leq r$ and $n(\Phi_V) \leq r$ conditions simultaneously. One can introduce even stronger constraints, e.g., $n_c - n(\Phi_C) + n(\Phi_V) \leq r$ which reduces further the electron transfer between C and V spaces. Note that in the following we use the latter condition

and set $r = 2$. Correspondingly, for the sake of compactness, we refer to the presented RAS-based method as DMRG-RAS.

The eigenvalue problem of the corresponding Hamiltonian projected from Eq. (1) by $\hat{P}_{RAS[r]}$ is written as

$$\hat{H}_{RAS[r]} \Psi_\alpha = \hat{P}_{RAS[r]} \hat{H} \hat{P}_{RAS[r]} \Psi_\alpha = E_\alpha \Psi_\alpha, \quad (4)$$

where $\Psi_\alpha \in \Phi_{RAS[r]}$ is the α -th many-body eigenstate of the projected Hamiltonian.

Considering a problem characterized by L_A , L_C , L_V number of active, restricted core and virtual spin-orbitals, respectively, at RAS[r] level of theory, the dimension of the associated Hilbert space scales as $\mathcal{O}(4^{L_A}(L_C + L_V)^r)$. Hence, diagonalizing large systems is challenged by the memory footprint of the Hamiltonian. In order to overcome this limitation, one viable strategy, proposed by the direct-CI approach,^{34,35} is to keep only slices of the matrix in memory during iterative diagonalization³⁶.

B. Schmidt decomposed RAS

As an alternative approach to the problem, hereby we propose a novel implementation of the RAS concept which takes advantage of the underlying direct product structure of the retained RAS configuration space. Namely, according to Eq. (3), the computational basis schematically consists of products of configuration states of set Φ_A and set $\Phi_{CV}^{(r)} \equiv \{\Phi_C\Phi_V \in \Phi_C\Phi_V | n_c - n(\Phi_C) + n(\Phi_V) \leq r\}$. It is worth to rewrite also the eigenvalue problem of Eq. (4) to emphasize the product structure,

$$\hat{H}_{\text{RAS}[r]} = \sum_i \hat{O}_A^{(i)} \otimes \hat{O}_{CV}^{(i)}$$

$$\Psi_\alpha = \sum_{\Phi_A \in \Phi_A \Phi_{CV} \in \Phi_{CV}^{(r)}} C_{\Phi_A \Phi_{CV}}^{(\alpha)} \Phi_A \Phi_{CV} \quad (5)$$

using coefficient matrix $C^{(\alpha)}$ and adequately constructed operators $\hat{O}_A^{(i)}$, $\hat{O}_{CV}^{(i)}$ acting on subspaces Φ_A and $\Phi_{CV}^{(r)}$, respectively. One major consequence of the bipartite representation³⁷ defined in Eq. 5 is that the consecutive states of the iterative diagonalization via Davidson or Lánczos algorithm, $\Psi' = \hat{H}_{\text{RAS}[r]}\Psi$, are obtained from the accumulated sum of product of matrices as

$$C^{(\alpha)'} = \sum_i O_A^{(i)} C^{(\alpha)} O_{CV}^{(i)T}. \quad (6)$$

Here, the dimension of the matrices reads as $|O_A| = [\mathcal{O}(4^{L_A}), \mathcal{O}(4^{L_A})]$, $|C_\alpha| = [\mathcal{O}(4^{L_A}), \mathcal{O}((L_C + L_V)^r)]$, $|O_{CV}| = [\mathcal{O}((L_C + L_V)^r), \mathcal{O}((L_C + L_V)^r)]$. Consequently for such a bipartite split, the memory requirement of each operator combination might be comparable to the footprint of the sliced-direct-CI method in the regime where $\mathcal{O}(4^{L_A}) \sim \mathcal{O}((L_C + L_V)^r)$. Note that the number of operator combinations is a quadratic function of L_A and $(L_C + L_V)$ for quantum chemical Hamiltonians. For more technical details of the representation see Refs. 38 and 39.

The active orbitals are represented by $\mathcal{O}(4^{L_A})$ number of states in the exact description. In order to reduce the computational demands, a truncated many-body basis set based on the Schmidt representation is proposed in the following.

III. NUMERICAL PROCEDURE

The Schmidt decomposed RAS representation can easily be adapted in the quantum chemical density matrix renormalization group (DMRG) approach^{39–44} through the dynamically extended active space (DEAS) procedure^{45,46} without additional programming efforts. In our implementation, the RAS concept was utilized within the Budapest-DMRG program package⁴⁷ using the so called two-site variant of DMRG, where the superblock is composed of the updated system block, two orbitals treated exactly and the environment block. In our representation, the system block extended with the two intermediate orbitals spans the configuration space of the active orbitals, Φ_A , and the environment block describes the restricted excitations on core and virtual orbitals, i.e., the corresponding subspace of $\Phi_{CV}^{(r)}$. The sweeping direction in the DMRG method can be reversed for any superblock configuration, thus we perform the sweeping only for the active orbital space and we leave the subspace of $\Phi_{\text{EXT}} \equiv \Phi_{CV}^{(r)}$ uncontracted. Since the size of the active block is always much smaller than the size of the environment block, partial summations to form the DMRG auxiliary operators are carried out for the environment block⁴³. The number of basis states used to represent $\Phi_{CV}^{(r)}$ is much larger than the dimension of a single orbital, thus the EXT orbital space kept fixed during the DMRG can also be considered as a super-site with large dimension attached to the right end of the DMRG chain.

From technical point of view, when the DEAS procedure is used, the left block contains one orbital from orbital set A in the first iteration step while the Hilbert spaces of the two intermediate sites together with the environment (right) are constructed from the remaining orbitals from set A and from subspaces of the C and V orbitals. The two intermediate sites are treated without any truncation while the right block basis states are formed with excitation rank up to $r = 2$. The nonzero matrix elements of the operators acting in the RAS space can be generated following the Slater-Condon rules^{48,49}. In the course of the forward sweep the size of the left block increased until the pre-set value of the CAS space is reached, and in each increment the left block basis is optimized via Schmidt decomposition^{29,43}. Therefore, the left-block is optimized via its interaction with the RAS space represented by the right block. At the end of the warmup procedure when the left block together with the two intermediate sites represent the desired number of A orbital set and the right block is formed only from the C and V orbital subspaces, the DMRG sweeping procedure is reversed. During the backward sweep the right block is optimized²⁹. In this embedding method, such sweeping procedure is repeated until convergence is reached, by keeping the number of retained basis states, also known as bond dimension, under control. In this work we used both fixed bond dimensions and dynamically adapted

values via the dynamical block state selection approach (DBSS)^{45,50} by setting an a priori error margin for the quantum information loss χ . In practice, a lower bound on the bond dimension, M_{\min} , is also enforced to boost convergence.

Note that RAS scheme can also be combined either with orbital optimization in a self-consistent manner or with perturbation theory to further improve the accuracy of the model.^{33,51} In our proof of concept implementation of the DMRG-RAS scheme we demonstrate in Sec. IV that high-quality solutions can be obtained even without such corrections just by treating large enough completely correlated active spaces. In addition, in a recent work⁵² some of us have proved and demonstrated by large-scale DMRG calculations that the DMRG-RAS energies obtained for increasing A spaces can be extrapolated to the FCI solution within chemical accuracy.

IV. RESULTS AND DISCUSSION

In the following, as proof of principle, various test calculations are presented for the strongly correlated C_2 and Cr_2 molecules. Ground state energies obtained with different standard quantum chemical methods are compared to the energy calculated by the RAS theory restricted up to two electron excitations ($r = 2$) denoted as DMRG-RAS in the following.

The Hartree–Fock electronic structure, multi-reference configuration interaction (MRCI), complete active space self-consistent field (CASSCF) and CASSCF referenced n -valence electron perturbation theory (NEVPT2) results are generated using quantum chemical program suite ORCA⁵³. High-level configuration interaction (CI) and coupled cluster expansion (CC) solutions as well as Hamiltonian matrix elements, required for the Budapest-DMRG code⁴⁷, are obtained by MRCC^{54,55}.

A. Proof of principle calculations - carbon dimer

The C_2 molecule is modeled at $d = 1.25$ Å bond length in frozen core cc-pVTZ basis⁵⁶ by correlating 4 electron pairs on 58 spatial-orbitals. In order to study the convergence of the RAS scheme towards the FCI energy as a function of gradually increasing subset A, a warmup DMRG calculation with DEAS is performed without truncation ($\chi = 0$) where the number of the completely correlated A orbitals is increased in each DMRG microiteration step. Note that in this benchmark, one molecular orbital (MO) with increasing energy is added to subspace A in each microiteration while the rest of the valence space is treated on the restricted level of theory permitting only at most two electron excitations from the reference HF configuration.

In Fig. 2 exact DMRG-RAS energies obtained for active spaces of increasing size ranging from $L_A = 3$ to 8 are presented in blue, where the character of the 8 MOs

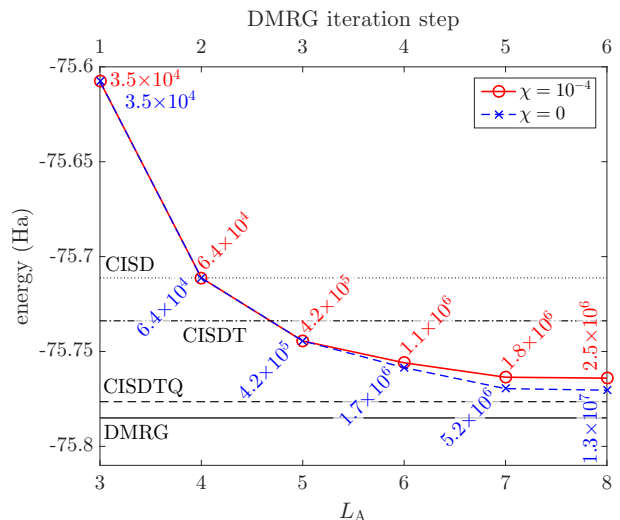


FIG. 2. Ground state energy of C_2 in frozen-core cc-pVTZ basis obtained by DMRG-RAS after the first half sweep for increasing L_A subspace using the DBSS truncation scheme. Dimension of the corresponding RAS configurational space is also shown besides the data points in the figure. The colored lines are guide to the eye. For comparison, reference CISD, CISDT, CISDTQ and large-scale DMRG energy levels are visualized by straight dotted, dashed-dotted, dashed and solid black lines, respectively. For more details of the computational test see Tab. I

in increasing energy order is identified as σ_{2s} , σ_{2s}^* , π_{2p_y} , π_{2p_z} , σ_{2p_x} , $\pi_{2p_y}^*$, $\pi_{2p_z}^*$, $\sigma_{2p_x}^*$. (The latter notation of x , y , z directions assumes that both C atoms are located in the x axis). In the first DMRG microiteration performed on the active space of $L_A = 3$ containing only occupied orbitals, i.e., σ_{2s} , σ_{2s}^* and π_{2p_y} , the DMRG-RAS solution corresponds to the CISD approximation by allowing up to two particle transfer between C and V by and applying the loose \mathcal{C} constrain defined in Sec. II A. Note that these equivalent solutions follow from the additional two-electron restriction on the space A formed purely of occupied orbitals. Applying the more restrictive constrain on the C and V spaces, a higher energy is obtained as shown in Fig. 2. For $L_A = 4$, where the restricted space includes exclusively virtual MOs, the CISD energy is predicted for both restriction constrains. We find that the energy drops significantly for $L_A = 5$ where the lowest lying unoccupied molecular orbital of σ_{2p_x} character is added to Φ_A configurational space which also indicates its strongly correlated character. The higher lying virtual orbitals incorporated in $L_A = 6, 7, 8$ active spaces, which all have positive orbital energy, affect less drastically the DMRG-RAS level of solution according to the many-body energy and the wave-function analysis.

By applying the DBSS truncation scheme, the exact ($\chi = 0$) RAS-space results can be approximated in order to reduce computational costs as depicted in Fig. 2 for truncation threshold $\chi = 10^{-4}$ and keeping $M_{\min} = 64$. In particular, for $L_A = 8$ the $M_{\text{exact}} = 4096$ states of the system block are represented by $M = 691$ many-

method	energy (Ha)	Δ_E (%)
HF	-75.4013	0.0
CASCI(8)	-75.5485	38.4
CASSCF(8)	-75.6386	61.8
CISD	-75.7112	80.8
CISDT	-75.7339	86.7
CISDTQ	-75.7765	97.8
MRCI(8)+Q	-75.7808	99.0
CCSD ^a	-75.7496	90.8
CCSD(T) ^a	-75.7832	99.5
CCSDT ^a	-75.7810	99.0
CCSDTQ ^a	-75.7845	99.9
NEVPT2(8) ^a	-75.7540	91.9
DMRG-RAS(8, $\chi = 10^{-4}$) ^b	-75.7640	94.5
DMRG-RAS(8, $\chi = 0$) ^b	-75.7704	96.2
DMRG-RAS(8, $M = 5051$)	-75.7704	96.2
DMRG-RAS(8, $M = 500$)	-75.7694	95.9
DMRG-RAS(8, $\chi = 10^{-4}$)	-75.7703	96.2
DMRG-RAS(14, $M = 500$)	-75.7753	97.5
DMRG-RAS(14, $\chi = 10^{-4}$)	-75.7792	98.5
DMRG-RAS(14, $\chi = 10^{-6}$)	-75.7809	99.0
DMRG-RAS(18, $M = 500$)	-75.7768	97.8
DMRG-RAS(18, $\chi = 10^{-4}$)	-75.7795	98.6
DMRG-RAS(18, $\chi = 10^{-6}$)	-75.7836	99.6
DMRG(58, $M = 500$)	-75.7779	98.1
DMRG(58, $\chi = 10^{-6}$)	-75.7849	99.9
DMRG(58, $M = 4096$)	-75.7850	100.0

TABLE I. Ground state energy of C_2 in cc-pVTZ basis using frozen-core approximation computed by various post-HF methods which correlate 8 electrons. For the active space methods the number of active orbitals are given in parenthesis while for the DMRG results the applied truncation scheme is also denoted. A series of standard DMRG calculations performed on the complete space of 58 orbitals is also included. Standard DMRG performed with retained 4096 block states provides the reference correlation energy. Δ_E stands for the percentage of correlation energy retrieved by the method. The superscript *a* denotes the non-variational solutions. The superscript *b* corresponds to energy obtained by the first half DMRG sweep, i.e., at the end of the DMRG warmup procedure.

body states and accordingly the total Hilbert space of the problem is also reduced by a factor of five. The introduced truncation yields an energy discrepancy in the range of 0.0 to 0.013 for increasing L_A (see also Tab. I).

Nevertheless, this error can be eliminated by performing DMRG sweeps restricted to the completely correlated orbital set *A*. As a proof-of-principle, retaining $M = 5051$ block states through the DMRG backward sweep the exact DMRG-RAS energy can be accurately reproduced by reaching the left turning point of the sweeping. Retaining fixed number of block states, $M = 500$, while the rank of the Hamiltonian in the effective subspace is two orders of magnitude smaller than the uncon-

tracted RAS problem, the exact result can be approached within an error of 1 mHa. Utilizing the DBSS procedure with $\chi = 10^{-4}$ and $M_{\min} = 64$ during the DMRG sweeping, in line with expectations, after a series of DMRG sweeps we get a converged energy with a marginal error of 0.1 mHa.

As a comparison, reference results of standard post-HF methods are also compiled in Tab. I and illustrated in Fig. 2. We find that although CASCI(8,8) result can be significantly lowered by SCF orbital optimization, it is still substantially higher than cheap CISD approximation due to its poor description of dynamical correlation effects. Modeling the problem at CISD, CISDT and CISDTQ level of theory, the retrieved correlation energy with respect to the reference DMRG correlation energy (obtained using $M = 4096$ and 58 orbitals) increases as 80.8%, 86.7%, 97.8%, respectively. Comparing to the single-reference CISD and CISDT solutions, DMRG-RAS yields higher resolution of correlations by construction already for $L_A = 5$ setup. On the other hand, setting against the standard DMRG energy, which considers all possible excitations without any restrictions, the DMRG-RAS solution is off by 0.022 Ha for $L_A = 8$ recovering 96.2% of the total correlation energy. Notable that CISDTQ provides practically exact solution retrieving 97.9% of the correlations. In Tab. I CC results of various complexity are presented as well. The data clearly demonstrates that the DMRG-RAS approach computed at modest active space size might not only outperform standard single-reference CI expansions but also cheap CC solutions, note that DMRG-RAS provides lower energy than CCSD already for $L_A = 6$. Furthermore, NEVPT2 results are also outperformed using DMRG-RAS level of theory. Even though the variational RAS based description is computationally more demanding compared to perturbation theory, it might provide more-reliable estimate for strongly correlated problems.

Increasing the size of completely correlated space *A*, the RAS energy decreases at a price of increasing computational efforts. As a demonstration, in Tab. I we also present DMRG-RAS energies obtained for *A* subspaces extended by virtuals selected according orbital energy. Describing sizeable active spaces, the basis truncation is already essential to keep the computations feasible. Retaining $M = 500$, we find that extending the 8 orbital active space with MOs of character σ_{3p_x} , π_{3p_y} , π_{3p_z} , σ_{3s} , $\pi_{3p_y}^*$ and $\pi_{3p_z}^*$, yielding $L_A = 14$ in total, the CISDTQ energy is recovered with an accuracy of 1 mHa. Applying the more precise DBSS truncation method with $\chi = 10^{-6}$, already CCSDT solution can be reached within 0.1 mHa. Furthermore, extending the active space to $L_A = 18$ orbitals with σ_{3s}^* , $\delta_{3d_{yz}}$, $\delta_{3d_{y^2-z^2}}$ and $\sigma_{3p_x}^*$ MOs, already CCSDTQ prediction can be retrieved within chemical accuracy.

1. Stretching the geometry

Next, we show that our approach is not restricted only to the equilibrium geometry but it can be applied through the whole potential energy surface (PES). Ground state energy of C_2 obtained by various post-HF methods for various interatomic distances, d , together with DMRG-RAS solutions are collected in Tab. II. It is clearly visible that even a very cheap DMRG-RAS($8, M = 500$) provides lower energy bounds compared to CCSD along the whole PES, while DMRG-RAS($18, M = 500$) is already comparable to CCSDT level of theory. Increasing the accuracy of the RAS(18) calculation by fixing the truncation error to $\chi = 10^{-6}$, good agreement is found with CCSDTQ calculated PES except for the most correlated setup at $d = 1.75 \text{ \AA}$, where DMRG-RAS predicts significantly lower energy. Note that MRCI(8) with Davidson Q correction consistently confirms the trends of the DMRG-RAS($18, \chi = 10^{-6}$) solution. In fact, MRCI(8)+Q predicts energy within chemical accuracy for large separations, $d \geq 2.75 \text{ \AA}$, while it provides $0.002 - 0.02 \text{ Ha}$ higher energies for moderate interatomic distances, $d < 2.75 \text{ \AA}$. Note also that DMRG-RAS method performed on a given A space is variational, thus increasing M or lowering χ provides a monotonic and stable convergence and even the cheap DMRG-RAS($8, M = 500$) gives a smooth PES. Therefore, for a fixed bond length no oscillations are experienced like in CC for $d = 3.25 \text{ \AA}$.

Based on the PES, experimentally measurable quantities - such as equilibrium bond length, r_e harmonic vibration frequency, ω_e , and dissociation energy, D_e , - can

method	$d \text{ (\AA)}$					
	1.25	1.75	2.25	2.75	3.25	5.00
CISD	-0.711	-0.568	-0.517	-0.440	-0.394	-0.368
CISDT	-0.734	-0.593	-0.541	-0.473	-0.451	-0.452
CISDTQ	-0.777	-0.660	-0.591	-0.553	-0.547	-0.550
MRCI(8)+Q	-0.781	-0.674	-0.599	-0.570	-0.564	-0.562
CCSD	-0.750	-0.613	-0.559	-0.513	-0.504	-0.334
CCSD(T)	-0.783	-0.654	-0.595	-0.581	-0.615	-0.498
CCSDT	-0.781	-0.654	-0.594	-0.576	-0.582	-0.424
CCSDTQ	-0.785	-0.651	-0.601	-0.573	-0.569	-0.570
CASSCF(8)	-0.639	-0.514	-0.444	-0.417	-0.413	-0.412
NEVPT2(8)	-0.754	-0.662	-0.576	-0.539	-0.534	-0.532
RAS(8) ^a	-0.769	-0.682	-0.587	-0.558	-0.551	-0.551
RAS(18) ^a	-0.777	-0.688	-0.593	-0.560	-0.555	-0.556
RAS(18) ^b	-0.784	-0.695	-0.601	-0.570	-0.563	-0.561

TABLE II. Potential energy surface of the C_2 molecule calculated for various interatomic distances d . The ground state energies obtained by different post-HF methods, measured in Ha, are shifted by 75.00 Ha and rounded to third digit resulting an error comparable to chemical accuracy. In case of superscript *a* DMRG-RAS calculations were performed with fixed $M = 500$, in case of superscript *b* the DBSS scheme with $\chi = 10^{-6}$ was used.

Method	$r_e \text{ (\AA)}$	$\omega_e \text{ (cm}^{-1}\text{)}$	$D_e \text{ (kcal/mol)}$
CCSD ¹⁷	1.240	1915	156.6
DMRG(8)-tCCSD ¹⁷	1.249	1885	146.3
MRCI ⁵⁷	1.252	1840	140.4
FCIQMC ⁵⁸	1.253	1835	135.4
DMRG-RAS(8)	1.255	1821	140.9
DMRG-RAS(18)	1.253	1839	135.8
Experiment ⁵⁹	1.243	1855	147.8

TABLE III. Spectroscopic constants for the dissociation of C_2 at different levels of theory in cc-pVTZ basis. Parameters r_e , ω_e and D_e denote equilibrium bond distance, harmonic vibration frequency and dissociation energy, respectively.

also be derived. Scanning the PES around the equilibrium, in the range of 1.235 \AA to 1.275 \AA , we found that our numerical data excellently fits the harmonic approximation. The DMRG-RAS dissociation energy, D_e , is derived from the energy of two carbon atoms computed at separation $d = 1000 \text{ \AA}$. The DMRG-RAS results together with benchmark results obtained by various others methods are presented in Tab. III. We find that the DMRG-RAS results depend slightly on the active space size, however, for $L_A = 18$ the high-level quantum Monte Carlo based FCIQMC reference data are reproduced already up to three digits. Note that experimental data, which is also included for completeness, is not expected to be precisely predicted by the numerical results owing to the limitations of the finite basis set and to the frozen core approximation.

Finally, recalling that the linear configurational interaction theory applied for a single reference is notorious for the lack of size-consistency⁶⁰. Here, we also investigate this open problem for the RAS description which essentially provides a multi-referenced CI solution. As a test, we compared the DMRG-RAS(18) energy obtained for C_2 separated by 1000 \AA , $E = -75.5606 \text{ Ha}$, and the twice of the DMRG-RAS energy for a single C atom keeping 9 orbitals in the active space, $E = 2 \times -37.7808 = -75.5616 \text{ Ha}$, which yields a discrepancy below chemical accuracy. Note that the accuracy of size-consistency in the RAS calculations can be controlled by the active space selection and the choice of basis, furthermore it can also be improved a posteriori by applying the Davidson correction⁶¹ or by implementing the quadratic CI theory⁶⁰. A more detailed analysis, also for more complex systems, is under progress and will be part of our subsequent work.

2. Convergence in large basis set

Numerical results obtained for C_2 at separation $d = 1.25 \text{ \AA}$ modeled in cc-pVQZ basis set with frozen cores are shown in Fig. 3 and also summarized in Tab. IV. Considering the extensive number of orbitals, $L = 108$, the

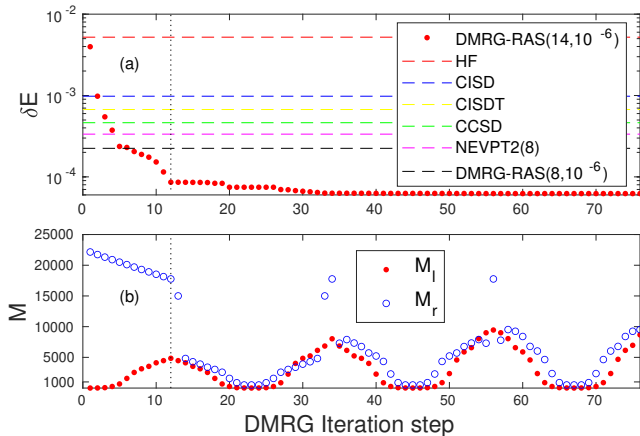


FIG. 3. (a) Relative error, δE , of the ground state energy with respect to the CCSD(T) reference energy, $E = -75.8007(\text{Ha})$, obtained by various standard methods and by the RAS-SD-DMRG for $L_A = 8, 14$ and $\chi = 10^{-6}$ and for cc-pVQZ basis corresponding to $L = 108$ orbitals. (b) For $L_A = 14$ the convergence profile as a function of DMRG iteration steps in terms of the corresponding number of the retained DMRG block states, M . Vertical dotted line indicates the last step of the first half DMRG sweep, i.e., at the end of the DMRG warmup procedure.

analysis is restricted to the computationally less demanding methods which confirms trends found in the smaller basis calculations.

Most notably, DMRG-RAS applied for active spaces of moderate size is already capable to outperform CISDT, CCSD and NEVPT2 energies after the first half DMRG sweep, see Tab. IV for $L_A = 8$ and Fig. 3 for $L_A = 14$. By carrying out sweepings for $L_A = 8$ with fixed $M = 500$ block states or by fixing $\chi = 10^{-6}$ the energy can be fur-

method	energy (Ha)
HF	-75.40561
CISD	-75.7264
CISDT	-75.7497
CCSD ^a	-75.7656
CCSD(T) ^a	-75.8007
NEVPT2(8) ^a	-75.7753
DMRG-RAS(8, $\chi = 10^{-6}$) ^b	-75.7749
DMRG-RAS(8, $M = 500$)	-75.7828
DMRG-RAS(8, $\chi = 10^{-6}$)	-75.7837
DMRG-RAS(14, $\chi = 10^{-6}$)	-75.7971

TABLE IV. Similar test calculations as in Tab. I, but for cc-pVQZ basis corresponding to $L = 108$ orbitals. The L_A number of completely correlated orbitals used in NEVPT2 and DMRG-RAS calculations are noted in parenthesis. For DMRG-RAS calculations the applied truncation criteria is also given. The superscript *a* and *b* denote the non-variational solutions and the energy obtained by the first half DMRG sweep (warmup procedure), respectively.

ther lowered significantly. In addition, increasing L_A to 14 the CCSD(T) reference energy can be reached within chemical accuracy. As shown in Fig. 3b, the tremendous drop in the number of retained block states after the first sweep demonstrates the efficiency of the DMRG basis state selection. Note that in case of computationally demanding problems, Φ_{CV} can also be included in the DMRG sweeping procedure with further constraints and an optimally selected Φ_{CV} space can be constructed according to quantum information entropies⁴⁵. For more complex systems, DMRG ordering optimization together with orbital optimization to provide more appropriate orbital set A can also be critical as will be shown below.

B. Optimization strategies for more complex systems - case study of chromium dimer

In the following, we study the performance of the DMRG-RAS approach for the strongly correlated chromium dimer which multi-reference problem is also often used to benchmark DMRG-based methods^{13,62–65}. Calculations are performed for the Cr_2 molecule in its equilibrium geometry, $d = 1.6788 \text{ \AA}$, in the cc-pVDZ atomic basis which model the correlation of the twelve $3d4s$ electrons in the space of 68 spin-orbitals while keeping all other lower-energy electrons frozen. The obtained post-HF results for the singlet and triplet lowest lying states are summarized in Tab. V

For the singlet state, we observe the relative low variance of the high-level CC reference data which might indicate a reliable convergence to the FCI solution. In contrast, the computation of the lowest triplet state by CI and CC methods is proven to be more challenging as will be shown below. Since single reference methods might depend heavily on the chosen reference determinant, we performed independent CC calculations by varying the SCF settings in the MRCC program package. In Tab. V, the lowest CI and CC energies, which were obtained by the default SCF setting, is shown. Being more sensitive to the reference determinant, we find that the triplet energy drops substantially for increasing model complexity contrary to the singlet case. Consequently, the singlet-triplet gap, expected to be around 1 eV⁶³, is significantly overestimated by the presented CI and CC solutions.

Turning the focus to the DMRG-RAS theory, we present several computational strategies which have the potential to improve systematically the convergence of the method. In the most naive computational scheme, we correlate 12 electrons on the 12 canonical orbitals around the HOMO-LUMO gap in active space A. The RAS theory provides only slightly lower energy than the standard CISD solution indicating the inadequacy of the virtual orbitals selected for subspace A, see DMRG-RAS energies with superscript *a* in Tab. V. Note that completely correlated subset of canonical orbitals is formed of the six bonding orbitals ($\sigma_{3d_{z^2}}$, σ_{4s} as well as the twofold degenerate π_{3d} and δ_{3d}) and the virtual orbitals with lowest

method	singlet (Ha)	triplet (Ha)	gap (eV)
CISD	-2086.5501	-2085.9127	17.34
CISDT	-2086.5932	-2086.2260	9.99
CCSD	-2086.7401	-2086.0758	18.08
CCSD(T)	-2086.8785	-2086.5059	10.14
CCSDT	-2086.8675	-2086.7042	4.44
CCSDTQ	-2086.8689	-2086.7282	3.83
CASSCF(12)	-2086.6502	-2086.6213	0.79
NEVPT2(12)	-2087.2744	-2087.2460	0.77
RAS(12, $M=500$) ^a	-2086.5626	-2086.5005	1.69
RAS(12, $M=500$) ^b	-2086.7686	-2086.7364	0.88
RAS(12, $M=500$) ^c	-2086.8516	-2086.8236	0.76
RAS(20, $M=500$) ^c	-2086.8542	-2086.8263	0.76
RAS(20, $M=1000$) ^c	-2086.8646	-2086.8359	0.78

TABLE V. Ground state energy of Cr₂ in its equilibrium geometry obtained by different post-HF methods in cc-pVDZ basis and frozen-core approximation. The correlation of the twelve 4s3d electrons are included explicitly by all the non-perturbative approaches. The L_A number of completely correlated orbitals used in CASSCF, NEVPT2 and DMRG-RAS calculations are noted in parenthesis. For DMRG-RAS calculations the number of retained block states M is also given. Superscripts *a* and *b* correspond to DMRG-RAS calculations performed on active orbitals selected from the canonical orbital set around the HOMO-LUMO gap or to the orbital entropy profile, respectively. The superscript *c* denotes DMRG-RAS results obtained in natural orbital basis, where the completely correlated orbitals were selected according to their chemical relevance reflected by large orbital entropies.

energies. We find that these MOs are composed of 4s and 4p atomic orbitals while the chemical intuition suggests that the relevant virtual orbitals are those antibonding MOs which correspond to bonding orbitals featuring 4s and 3d atomic orbitals. This assumption is also corroborated by studying the single orbital entropy profile^{45,66} of the molecule to identify the relevant orbitals, which

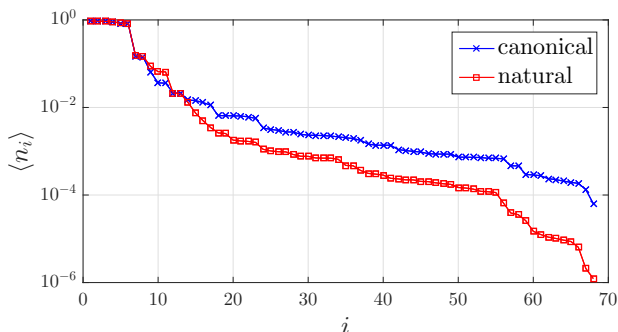


FIG. 4. Sorted orbital occupation calculated by a low-accuracy ($M = 300$) DMRG for the ground state of the chromium dimer obtained in the canonical orbital and in the corresponding natural orbital basis set. The solid lines are guides to the eye.

we obtained from a low-precision ($M = 300$) standard DMRG calculation on the complete space of 68 orbitals. Accordingly, by choosing the six chemically most relevant antibonding 4s and 3d virtual orbitals in subspace A, the DMRG-RAS energy drops drastically and gets even below the CCSD reference energy (see superscript *b* in Tab. V).

In order to further improve the DMRG-RAS energy, we recall that the restricted excitations of the RAS space could only represent those orbitals faithfully whose chemical importance is negligible, i.e., orbitals with occupation number close to zero or two. Accordingly, by expressing the Hamiltonian in the natural orbital basis based on a low-precision ($M = 300$) DMRG calculation, orbitals with larger partial occupation are concentrated only on a few number of virtual orbitals and the rest of the spectrum has a much faster decay compared to the one obtained for canonical orbitals, see Fig. 4. Utilizing the natural orbitals in the DMRG-RAS method with $L_A = 12$ active orbitals the CCSDT energy can be recovered up to 0.016 Ha, see RAS data indicated by superscript *c* in Tab. V. Furthermore, using the same strategy but extending the completely correlated subspace A by keeping $L_A = 20$ orbitals, the CCSDT ground state energy is reproduced practically up to chemical accuracy (0.003 Ha).

Repeating the same analysis for the lowest-lying triplet state the DMRG-RAS provides again a stable and monotonic convergence with increasing L_A and M values. Using natural orbitals the calculated gap shows only very small variance for increasing L_A and M values. It is also remarkable that even though CASSCF, NEVPT2 and high-level DMRG-RAS report substantially different absolute energies, all these three methods predict energy gap around 0.78 eV which result is also in line with previous findings⁶³. Note that the lowest absolute energies of the NEVPT2 solution, which retrieves correlation effects of the core electrons in a perturbative manner, imply the relevance of lower-energy 3s3p electrons for a reliable description of the chromium dimer.

V. CONCLUSIONS

In this work, we proposed a formulation of the restricted active space scheme considering the Schmidt decomposition which can be efficiently treated by the density matrix renormalization group method through the dynamically extended active space (DEAS) procedure without additional programming efforts. The dimension of the Hilbert space of the uncontracted RAS orbital space can easily be chosen to be in the range of a few tens of thousands also taking into account the sparsity of the corresponding matrices. The iterative decomposition also provides a possibility to truncate the Hilbert space of the active orbital space using quantum information measures. Most importantly, optimization of the CAS space is carried out in the presence of the EXT

space, unlike in case of other embedding methods. As a proof of concept, we tested the method dubbed DMRG-RAS on the strongly correlated problem of carbon and chromium dimers which is compared to standard state-of-the-art numerical solutions rivaling with respect to accuracy and computational demand. Our method is variational and provides a stable and monotonic convergence with increasing size of the active space and DMRG bond dimension not only at equilibrium geometries, but along the whole potential energy surface even when multireference character gets more pronounced. When lowest lying excited states are targeted in different quantum number sectors similar properties hold. The performance of the DMRG-RAS method can be further boosted by basis optimization and utilization of concepts of quantum information theory. The generalization of the presented computational scheme as a multilayered protocol is straightforward where most RAS orbitals are treated only up to double excitation level while the more intricate ones are at higher level of theory. The method is expected to be particularly well-suited to provide a balanced description of static and dynamical correlations of ab initio systems with orbital space separable according to its correlation pattern.

While completing our work we got aware of a similar approach⁶⁷ suggesting to attach large sites to the two ends of the DMRG chain. A more detailed analysis of excited states together with improving the CC approach via DMRG-RAS is part of our current work.

ACKNOWLEDGMENTS

This work was supported by the Ministry of Innovation and Technology and the National Research, Develop-

ment and Innovation Office of Hungary (NKFIH) within the Quantum Information National Laboratory of Hungary and project No. K134983, No. TKP2021-NVA-04 and No. FK-135496. M.A.W. has also been supported by the ÚNKP-21-4 and NKP-22-5-BME-330 New National Excellence Program of the Ministry for Culture and Innovation from the source of the National Research, Development and Innovation Fund. The Bolyai Research Scholarship of HAS is greatly acknowledged by G.B. and M.A.W. We acknowledge KIFÜ for awarding us access to computational resource based in Hungary. T.S. would like to thank the University of Alabama and the Office of Information Technology for providing high performance computing resources and support that have contributed to these research results. This work was made possible in part by a grant of high-performance computing resources and technical support from the Alabama Supercomputer Authority. Ö.L. also acknowledges financial support from the Hans Fischer Senior Fellowship programme funded by the Technical University of Munich – Institute for Advanced Study. The development of DMRG libraries has been supported by the Center for Scalable and Predictive methods for Excitation and Correlated phenomena (SPEC), which is funded as part of the Computational Chemical Sciences Program by the U.S. Department of Energy (DOE), Office of Science, Office of Basic Energy Sciences, Division of Chemical Sciences, Geosciences, and Biosciences at Pacific Northwest National Laboratory.

Dedicated to the memory of Géza Tichy and János Pipek.

* legeza.ors@wigner.hu

¹ Szabo, A.; Ostlund, N. S. *Modern Quantum Chemistry: Introduction to Advanced Electronic Structure Theory*, 1st ed.; Dover Publications, Inc.: Mineola, 1996

² Vogiatzis, K. D.; Ma, D.; Olsen, J.; Gagliardi, L.; de Jong, W. A. Pushing configuration-interaction to the limit: Towards massively parallel MCSCF calculations. *The Journal of Chemical Physics* **2017**, *147*, 184111

³ Roos, B. O. *Advances in Chemical Physics*; John Wiley and Sons, Ltd, 1987; pp 399–445

⁴ Cramer, C. *Essentials of Computational Chemistry: Theories and Models*; Wiley, 2005

⁵ Jensen, F. *Introduction to Computational Chemistry*; John Wiley and Sons, Inc.: Hoboken, NJ, USA, 2006

⁶ Becke, A. D. Density functionals for static, dynamical, and strong correlation. *The Journal of Chemical Physics* **2013**, *138*, 074109

⁷ Benavides-Riveros, C. L.; Lathiotakis, N. N.; Marques, M. A. L. Towards a formal definition of static and dynamic electronic correlations. *Phys. Chem. Chem. Phys.* **2017**, *19*, 12655–12664

⁸ Olsen, J. The CASSCF method: A perspective and commentary. *International Journal of Quantum Chemistry* **2011**, *111*, 3267–3272

⁹ Kinoshita, T.; Hino, O.; Bartlett, R. J. Coupled-cluster method tailored by configuration interaction. *The Journal of Chemical Physics* **2005**, *123*, 074106

¹⁰ Piecuch, P.; Tobol/a, R.; Paldus, J. Approximate account of connected quadruply excited clusters in single-reference coupled-cluster theory via cluster analysis of the projected unrestricted Hartree-Fock wave function. *Phys. Rev. A* **1996**, *54*, 1210–1241

¹¹ Kinoshita, T.; Hino, O.; Bartlett, R. J. Coupled-cluster method tailored by configuration interaction. *The Journal of Chemical Physics* **2005**, *123*, 074106

¹² Hino, O.; Kinoshita, T.; Chan, G. K.-L.; Bartlett, R. J. Tailored coupled cluster singles and doubles method applied to calculations on molecular structure and harmonic vibrational frequencies of ozone. *The Journal of Chemical Physics* **2006**, *124*, 114311

¹³ Veis, L.; Antalík, A.; Brabec, J.; Neese, F.; Legeza, Ö.; Pittner, J. Coupled Cluster Method with Single and Double

- Excitations Tailored by Matrix Product State Wave Functions. *The Journal of Physical Chemistry Letters* **2016**, *7*, 4072–4078
- ¹⁴ Lyakh, D. I.; Lotrich, V. F.; Bartlett, R. J. The ‘tailored’ CCSD(T) description of the automerization of cyclobutadiene. *Chemical Physics Letters* **2011**, *501*, 166–171
- ¹⁵ Melnichuk, A.; Bartlett, R. J. Relaxed active space: Fixing tailored-CC with high order coupled cluster. I. *The Journal of Chemical Physics* **2012**, *137*, 214103
- ¹⁶ Morchen, M.; Freitag, L.; Reiher, M. Tailored coupled cluster theory in varying correlation regimes. *The Journal of Chemical Physics* **2020**, *153*, 244113
- ¹⁷ Leszczyk, A.; Mate, M.; Legeza, O.; Boguslawski, K. Assessing the Accuracy of Tailored Coupled Cluster Methods Corrected by Electronic Wave Functions of Polynomial Cost. *Journal of Chemical Theory and Computation* **2022**, *18*, 96–117, PMID: 34965121
- ¹⁸ Faulstich, F. M.; Laestadius, A.; Legeza, Ö.; Schneider, R.; Kvaal, S. Analysis of the Tailored Coupled-Cluster Method in Quantum Chemistry. *SIAM Journal on Numerical Analysis* **2019**, *57*, 2579–2607
- ¹⁹ Faulstich, F. M.; Mate, M.; Laestadius, A.; Csirik, M. A.; Veis, L.; Antalik, A.; Brabec, J.; Schneider, R.; Pittner, J.; Kvaal, S.; Legeza, Ö. Numerical and Theoretical Aspects of the DMRG-TCC Method Exemplified by the Nitrogen Dimer. *Journal of Chemical Theory and Computation* **2019**, *15*, 2206–2220
- ²⁰ Tecmer, P.; Boguslawski, K. Geminal-based electronic structure methods in quantum chemistry. Toward a geminal model chemistry. *Phys. Chem. Chem. Phys.* **2022**, *24*, 23026–23048
- ²¹ Jeziorski, B. Multireference coupled-cluster Ansatz. *Molecular Physics* **2010**, *108*, 3043–3054
- ²² Lyakh, D. I.; Musial, M.; Lotrich, V. F.; Bartlett, R. J. Multireference Nature of Chemistry: The Coupled-Cluster View. *Chemical Reviews* **2012**, *112*, 182–243, PMID: 22220988
- ²³ Evangelista, F. A. Perspective: Multireference coupled cluster theories of dynamical electron correlation. *The Journal of Chemical Physics* **2018**, *149*, 030901
- ²⁴ Lischka, H.; Nachtigallova, D.; Aquino, A. J. A.; Szalay, P. G.; Plasser, F.; Machado, F. B. C.; Barbatti, M. Multireference Approaches for Excited States of Molecules. *Chemical Reviews* **2018**, *118*, 7293–7361
- ²⁵ Fleig, T.; Olsen, J.; Marian, C. M. The generalized active space concept for the relativistic treatment of electron correlation. I. Kramers-restricted two-component configuration interaction. *The Journal of Chemical Physics* **2001**, *114*, 4775–4790
- ²⁶ Ma, D.; Li Manni, G.; Gagliardi, L. The generalized active space concept in multiconfigurational self-consistent field methods. *The Journal of Chemical Physics* **2011**, *135*, 044128
- ²⁷ Olsen, J.; Roos, B. O.; Jorgensen, P.; Jensen, H. J. A. Determinant based configuration interaction algorithms for complete and restricted configuration interaction spaces. *The Journal of Chemical Physics* **1988**, *89*, 2185–2192
- ²⁸ Casanova, D. Restricted active space configuration interaction methods for strong correlation: Recent developments. *WIREs Computational Molecular Science* **2022**, *12*, e1561
- ²⁹ White, S. R. Density matrix formulation for quantum renormalization groups. *Phys. Rev. Lett.* **1992**, *69*, 2863–2866
- ³⁰ Parker, S. M.; Seideman, T.; Ratner, M. A.; Shiozaki, T. Communication: Active-space decomposition for molecular dimers. *The Journal of Chemical Physics* **2013**, *139*, 021108
- ³¹ Parker, S. M.; Shiozaki, T. Quasi-diabatic States from Active Space Decomposition. *Journal of Chemical Theory and Computation* **2014**, *10*, 3738–3744, PMID: 26588519
- ³² Nishio, S.; Kurashige, Y. Rank-one basis made from matrix-product states for a low-rank approximation of molecular aggregates. *The Journal of Chemical Physics* **2019**, *151*, 084110
- ³³ Malmqvist, P. A.; Rendell, A.; Roos, B. O. The restricted active space self-consistent-field method, implemented with a split graph unitary group approach. *The Journal of Physical Chemistry* **1990**, *94*, 5477–5482
- ³⁴ Roos, B. O.; Siegbahn, P. *Methods of Electronic Structure Theory. Modern Theoretical Chemistry, vol 3*; Springer: Boston, 1977
- ³⁵ Olsen, J.; Jorgensen, P.; Simons, J. Passing the one-billion limit in full configuration-interaction (FCI) calculations. *Chemical Physics Letters* **1990**, *169*, 463–472
- ³⁶ Davidson, E. R. The iterative calculation of a few of the lowest eigenvalues and corresponding eigenvectors of large real-symmetric matrices. *Journal of Computational Physics* **1975**, *17*, 87–94
- ³⁷ Horodecki, R.; Horodecki, P.; Horodecki, M.; Horodecki, K. Quantum entanglement. *Rev. Mod. Phys.* **2009**, *81*, 865–942
- ³⁸ Xiang, T. Density-matrix renormalization-group method in momentum space. *Phys. Rev. B* **1996**, *53*, R10445–R10448
- ³⁹ White, S. R.; Martin, R. L. Ab initio quantum chemistry using the density matrix renormalization group. *The Journal of Chemical Physics* **1999**, *110*, 4127–4130
- ⁴⁰ Yanai, T.; Kurashige, Y.; Ghosh, D.; Chan, G. K.-L. Accelerating convergence in iterative solution for large-scale complete active space self-consistent-field calculations. *International Journal of Quantum Chemistry* **2009**, *109*, 2178–2190
- ⁴¹ Chan, G. K.-L.; Sharma, S. The Density Matrix Renormalization Group in Quantum Chemistry. *Annual Review of Physical Chemistry* **2011**, *62*, 465–481, PMID: 21219144
- ⁴² Wouters, S.; Poelmans, W.; Ayers, P. W.; Neck, D. V. CheMPS2: A free open-source spin-adapted implementation of the density matrix renormalization group for ab initio quantum chemistry. *Computer Physics Communications* **2014**, *185*, 1501 – 1514
- ⁴³ Szalay, Sz.; Pfeffer, M.; Murg, V.; Barcza, G.; Verstraete, F.; Schneider, R.; Legeza, Ö. Tensor product methods and entanglement optimization for ab initio quantum chemistry. *Int. J. Quantum Chem.* **2015**, *115*, 1342–1391
- ⁴⁴ Baiardi, A.; Reiher, M. The density matrix renormalization group in chemistry and molecular physics: Recent developments and new challenges. *The Journal of Chemical Physics* **2020**, *152*, 040903
- ⁴⁵ Legeza, Ö.; Sólyom, J. Optimizing the density-matrix renormalization group method using quantum information entropy. *Phys. Rev. B* **2003**, *68*, 195116
- ⁴⁶ Barcza, G.; Legeza, Ö.; Marti, K. H.; Reiher, M. Quantum-information analysis of electronic states of different molecular structures. *Phys. Rev. A* **2011**, *83*, 012508
- ⁴⁷ Legeza, Ö.; Veis, L.; Mosoni, T. QC-DMRG-Budapest, a program for quantum chemical DMRG calculations
- ⁴⁸ Slater, J. C. The Theory of Complex Spectra. *Phys. Rev.* **1929**, *34*, 1293–1322

- ⁴⁹ Condon, E. U. The Theory of Complex Spectra. *Phys. Rev.* **1930**, *36*, 1121–1133
- ⁵⁰ Legeza, Ö.; Sólyom, J. Quantum data compression, quantum information generation, and the density-matrix renormalization-group method. *Phys. Rev. B* **2004**, *70*, 205118
- ⁵¹ Malmqvist, P. A.; Pierloot, K.; Shahi, A. R. M.; Cramer, C. J.; Gagliardi, L. The restricted active space followed by second-order perturbation theory method: Theory and application to the study of CuO₂ and Cu₂O₂ systems. *The Journal of Chemical Physics* **2008**, *128*, 204109
- ⁵² Friesecke, G.; Barcza, G.; Legeza, O. Predicting the FCI energy of large systems to chemical accuracy from restricted active space density matrix renormalization group calculations. 2022; <https://arxiv.org/abs/2209.14190>
- ⁵³ Neese, F. The ORCA program system. *WIREs Computational Molecular Science* **2012**, *2*, 73–78
- ⁵⁴ Kallay, M. et al. Mrcc, a quantum chemical program suite. 2020; www.mrcc.hu
- ⁵⁵ Kallay, M. et al. The MRCC program system: Accurate quantum chemistry from water to proteins. *The Journal of Chemical Physics* **2020**, *152*, 074107
- ⁵⁶ Dunning, T. H. Gaussian basis sets for use in correlated molecular calculations. I. The atoms boron through neon and hydrogen. *The Journal of Chemical Physics* **1989**, *90*, 1007–1023
- ⁵⁷ Peterson, K. A. Accurate multireference configuration interaction calculations on the lowest $1\Sigma^+$ and 3Π electronic states of C₂, CN⁺, BN, and BO⁺. *The Journal of Chemical Physics* **1995**, *102*, 262–277
- ⁵⁸ Booth, G. H.; Cleland, D.; Thom, A. J. W.; Alavi, A. Breaking the carbon dimer: The challenges of multiple bond dissociation with full configuration interaction quantum Monte Carlo methods. *The Journal of Chemical Physics* **2011**, *135*, 084104
- ⁵⁹ Huber, K. P.; Herzberg, G. *Molecular Spectra and Molecular Structure: IV. Constants of Diatomic Molecules*; Springer US: Boston, MA, 1979; pp 8–689
- ⁶⁰ Pople, J. A.; Head-Gordon, M.; Raghavachari, K. Quadratic configuration interaction. A general technique for determining electron correlation energies. *The Journal of Chemical Physics* **1987**, *87*, 5968–5975
- ⁶¹ Langhoff, S. R.; Davidson, E. R. Configuration interaction calculations on the nitrogen molecule. *International Journal of Quantum Chemistry* **1974**, *8*, 61–72
- ⁶² Kurashige, Y.; Yanai, T. Second-order perturbation theory with a density matrix renormalization group self-consistent field reference function: Theory and application to the study of chromium dimer. *The Journal of Chemical Physics* **2011**, *135*, 094104
- ⁶³ Sharma, S.; Chan, G. K.-L. Spin-adapted density matrix renormalization group algorithms for quantum chemistry. *The Journal of Chemical Physics* **2012**, *136*, 124121
- ⁶⁴ Ma, Y.; Knecht, S.; Keller, S.; Reiher, M. Second-Order Self-Consistent-Field Density-Matrix Renormalization Group. *Journal of Chemical Theory and Computation* **2017**, *13*, 2533–2549, PMID: 28485978
- ⁶⁵ Larsson, H. R.; Zhai, H.; Umrigar, C. J.; Chan, G. K.-L. The Chromium Dimer: Closing a Chapter of Quantum Chemistry. *Journal of the American Chemical Society* **2022**, *144*, 15932–15937
- ⁶⁶ Stein, C. J.; Reiher, M. Automated Selection of Active Orbital Spaces. *Journal of Chemical Theory and Computation* **2016**, *12*, 1760–1771, PMID: 26959891
- ⁶⁷ Larsson, H. R.; Zhai, H.; Gunst, K.; Chan, G. K.-L. Matrix product states with large sites. **2021**,